Supplement (part 1 of 2)

S1 Methods

S1.1 Study sites

Variable	n
DO_{mean}	140
DO_{min}	108
ln(conductivity)	143
ln(Depth)	169
ln(SA/D)	165
ln(Volume)	165
MAF	182
MAT	182
MST	178
WMT	177
pH	154
SWI	179

Table S1. Number of samples (n) with data for each environmental variable in the dataset.

	MAF (°C)	**pH**	**ln(Conductivity)**	**DO_{mean} (mg/L)**	**DO_{min} (mg/L)**	**ln(Depth)**	**ln(SA/D)**	**ln(Volume)**
MAF (°C)	1.00							
pH	0.60	1.00						
ln(Conductivity)	0.70	0.75	1.00					
DO mean (mg/L)	-0.57	-0.16	-0.17	1.00				
DO min (mg/L)	-0.43	0.10	-0.14	0.78	1.00			
ln(Depth)	0.05	0.03	0.13	-0.25	-0.37	1.00		
ln(SA/D)	0.27	0.57	0.55	0.40	0.47	-0.23	1.00	
ln(Volume)	0.30	0.56	0.60	0.20	0.18	0.45	0.77	1.00

Table S2. Correlation coefficients (*r*) between environmental parameters in the study dataset.

S1.2 Comparison of ASE and BD Methods

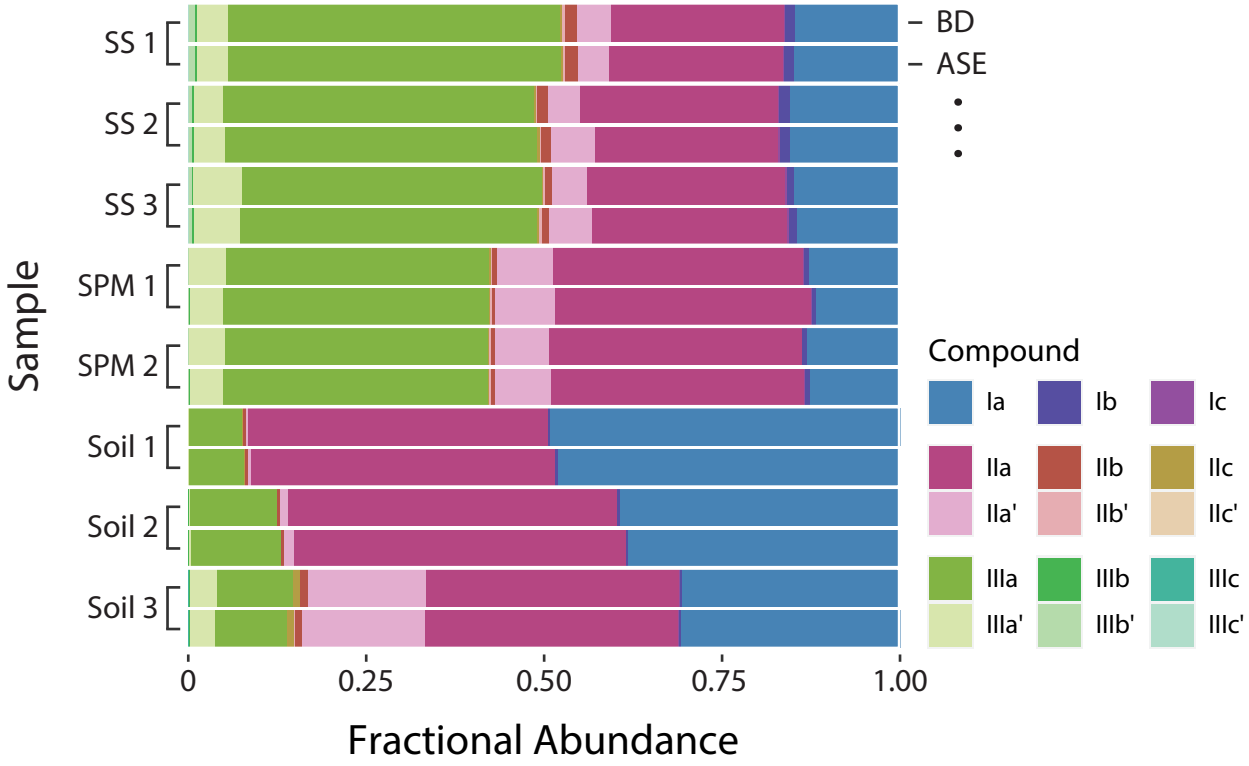

Figure S1. Comparison of fractional abundances (Full set) obtained using the Bligh and Dyer (BD; top of each pair) and accelerated solvent extractor (ASE; bottom of each pair) extraction methods. "SS" = Surface Sediment; "SPM" = Suspended Particulate Matter.

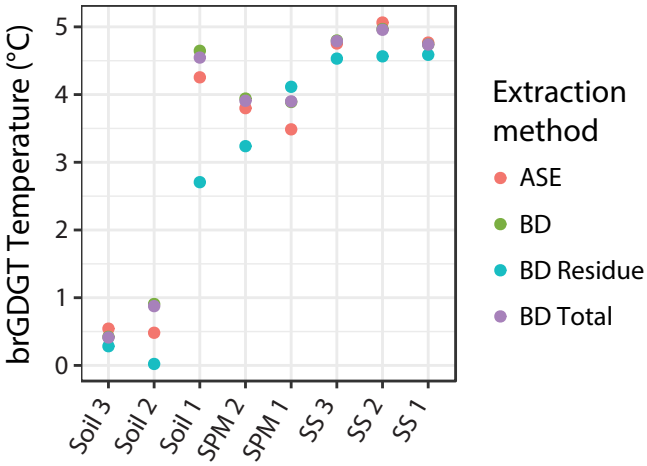

Figure S2. Comparison of brGDGT-derived temperatures obtained from samples extracted with the accelerated solvent extractor (ASE) and Bligh and Dyer (BD) extraction methods. The BD sample residue re-extracted with ASE ("BD Residue") and the sum of the BD and BD Residue samples ("BD Total") are additionally shown. Mean annual temperature for soil and lake samples were calculated using the Russell et al. (2018) and Naafs et al. (2017) MBT'$_{5Me}$ calibrations, respectively. "SS" = Surface Sediment; "SPM" = Suspended Particulate Matter.

S1.3 Comparison of WorldClim and logger temperatures

WorldClim- and iButton-derived climate normals were within one standard deviation for all months except June and July, for which the *in situ* logger temperatures were 1.0 ± 0.7 °C and 1.3 ± 1.0 °C higher, respectively. These warmer summer temperatures were most pronounced for sites sitting within deep glacial valleys, where high (> 100m) exposed rock walls may make them susceptible to warmer summer microclimates.

S1.4 Statistical and Analytical Methods

We treated compounds below the detection limit as having an absolute abundance of zero. This assumption led some sites to have compounds with FA = 0 and/or FA = 1. All of these FAs are plotted as such (e.g. Fig. 7c) and tend to be associated with noisier trends (presumably due in part to the lower abundances). Removing these sites from the dataset would have removed valuable points from the stronger trends (e.g. Fig. 7a), upon which our calibrations primarily rely. For subset-specific calibrations (e.g. Eqns. S1-S9), we did not face this issue and removed samples with any FA = 1.

S3 C5 versus C6 methylation

To the best of our knowledge, no experiments that model or probe brGDGT membrane properties currently exist. However, fluidity gradients have been shown to exist across other lipid membranes, with fluidity increasing from the membrane surface towards its interior (cf. Stillwell, 2016). In brGDGTs, the fluidity at carbon 6 might then be expected to be greater than at carbon 5. A methylation at the more rigid C5 position could therefore have a greater impact on membrane fluidity than one at C6, as it is positioned closer to the membrane's exterior. This hypothesis is consistent with our results, which show a slightly stronger temperature response in 5-methyl compounds compared to their 6-methyl counterparts on average (Figs. S6 and S7), though other explanations may certainly exist.

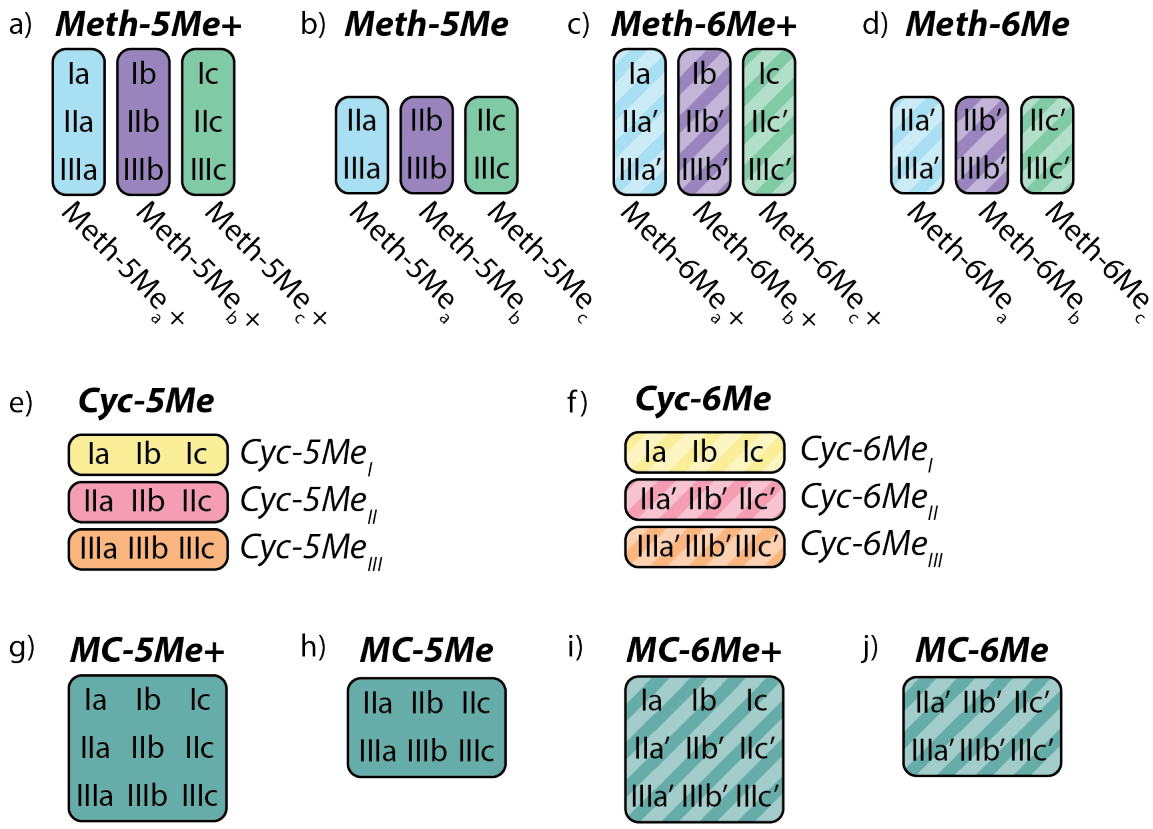

Figure S3. Structural subsets within the Meth (a-d), Cyc (e-f), and Meth-Cyc (MC; g-j) sets. Variations on the Meth and MC subsets that include (a, c, e, g) or exclude (b, d, f, h) tetramethylated compounds are shown. The complete Meth set (Fig. 2a) is composed of the Meth-5Me+ (a) and Meth-6Me (d) subsets. The complete MC set shown in (Fig. 2f) is composed of the MC-5Me+ (e) and MC-6Me (h) subsets.

Plots of the structural subset variations against MAF are additionally provided in the supplement_pt2.html file (Figs. S4-11).

S4 Structural Set Plots

Plots of all structural sets against MAF, conductivity, pH, and DO_{mean} are provided in the supplement_pt2.html file (Figs. S11-40).

S5 Calibration Results

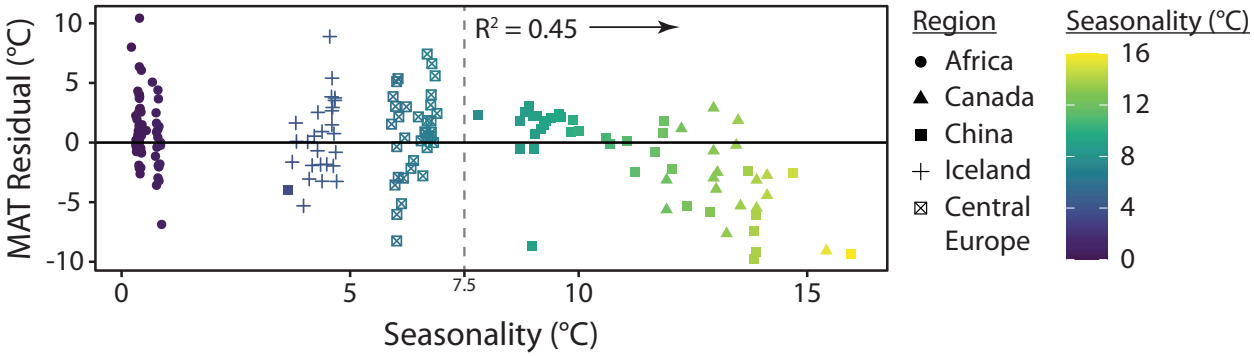

Figure S40. Residuals of the highest-performing fit (Meth set) for mean annual temperature (MAT) plotted against seasonality. The residuals correlate with seasonality (R2 = 0.14), especially when seasonality > 7.5 °C (R2 = 0.45).

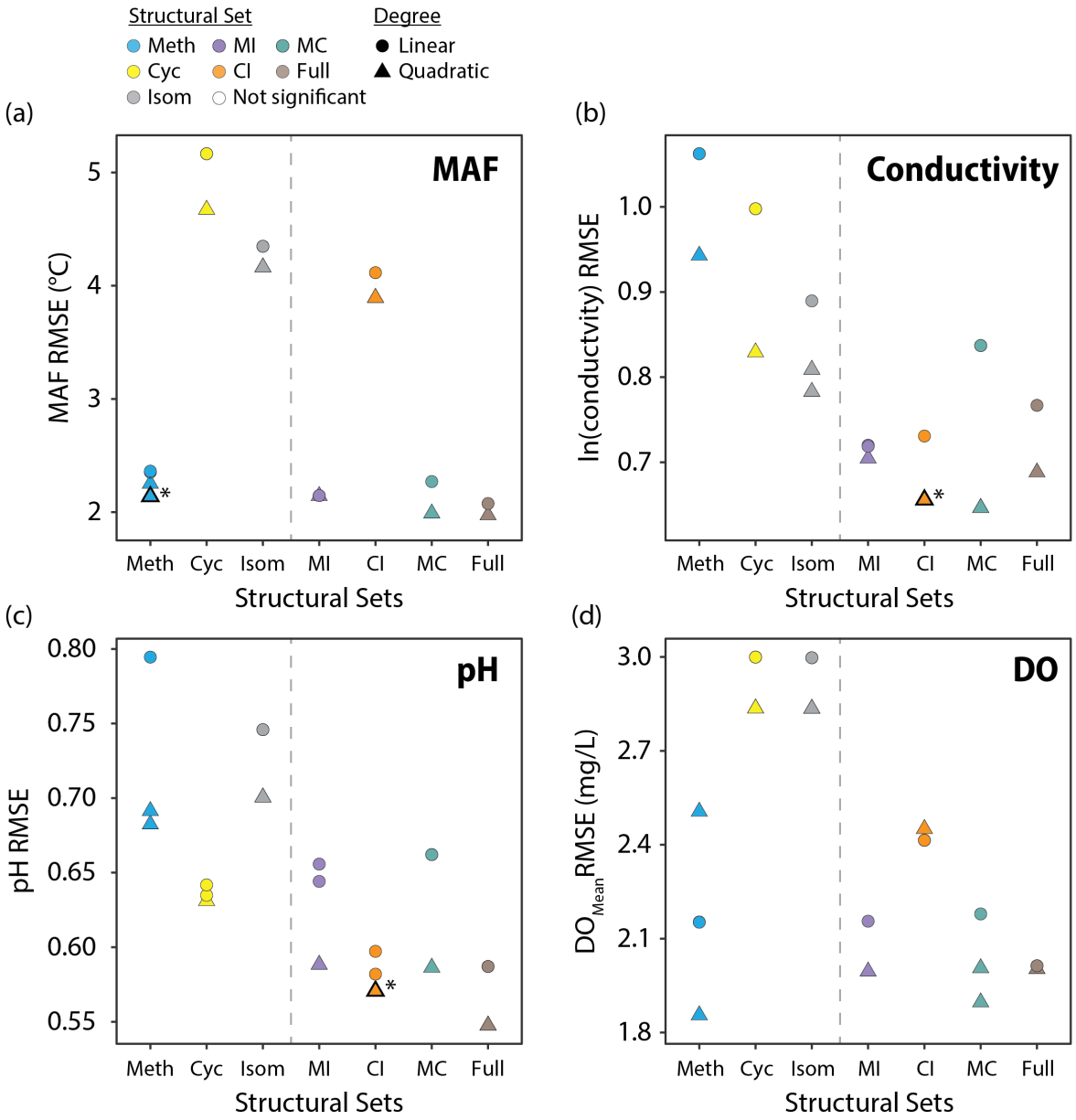

Figure S41. Performance (RMSE) of all linear and quadratic fits for a) the mean air temperature of months above freezing (MAF), b) conductivity, c) pH, and d) DO_{mean} and brGDGT fractional abundances (FAs) calculated within the basic (Meth, Cyc, Isom; left of dashed line) and combined (Meth-Isom (MI), Cyc-Isom (CI), Meth-Cyc (MC), and Full; right of dashed line) structural sets. Results of both the SFS/SBE and combinatoric fitting methods are plotted. The fit we suggest for general use (Meth set, quadratic, SFS/SBE; Eq. 10) is bolded and marked with an asterisk in a) and plotted in b). "Est. MAF" is the MAF temperature estimated using this suggested fit.

S5.1 Dissolved Oxygen

None of the DO or lake geometry variables generated strong brGDGT calibrations ($R^2 \leq 0.63$; Table S1). The highest-performing fit was provided by the Meth set with DO_{mean} ($R^2 = 0.63$, Figs. S42 and S41d). Moderate correlations were found with DO_{min} as well (Cyc set, $R^2 = 0.55$). Lake depth alone was a poor predictor of brGDGT distributions ($R^2 = 0.35$), but both volume and the ratio of surface area to depth were found to provide moderate correlations ($R^2 = 0.55$ and 0.59, respectively). However, none of these lake morphology variables was itself well-correlated with DO_{mean} or DO_{min} ($R^2 \leq 0.22$) in this dataset, and we therefore cannot explain their relationship with brGDGTs at this time. Additionally, although the ratio of 5-methyl hexamethylated to pentamethylated brGDGTs (HP5 index, Eq. A13) was recently shown to reflect redox conditions via a correlation with lake water depth (Yao et al., 2020), it does not correlate with any of our lake geometry indices ($R^2 \leq 0.02$) and only weakly correlates with DO ($R^2 \leq 0.28$) in this dataset, indicating that it may be primarily useful for within-lake studies.

The Meth set provided both the strongest DO_{mean} and MAF calibrations, raising the possibility that DO may have a problematic influence on that calibration's temperature estimates. Individual Meth FAs were weakly correlated with DO_{mean} at best ($R^2 \leq 0.35$), however, and the residuals of the Meth/MAF fit in Eq. 10 showed no correlation with DO_{mean} ($R^2 = 0.01$, $p = 0.2$). Furthermore, DO was somewhat correlated with MAF in our dataset ($r = -0.57$), indicating that it may not be possible to separate these variables fully in this study. Given these weak relationships, we do not see evidence for the influence of DO on temperatures reconstructed with the Meth calibration in our dataset.

Overall, dissolved oxygen and lake geometry calibrations generated significant, but statistically weaker fits ($R^2 \leq 0.63$). Due to the low R^2 of these calibrations and an incomplete understanding of the relationship between DO and brGDGT distributions, we do not recommend their application at this time. However, the equation for the highest-performing variable, DO_{mean}, is provided for reference (Eq. S11).

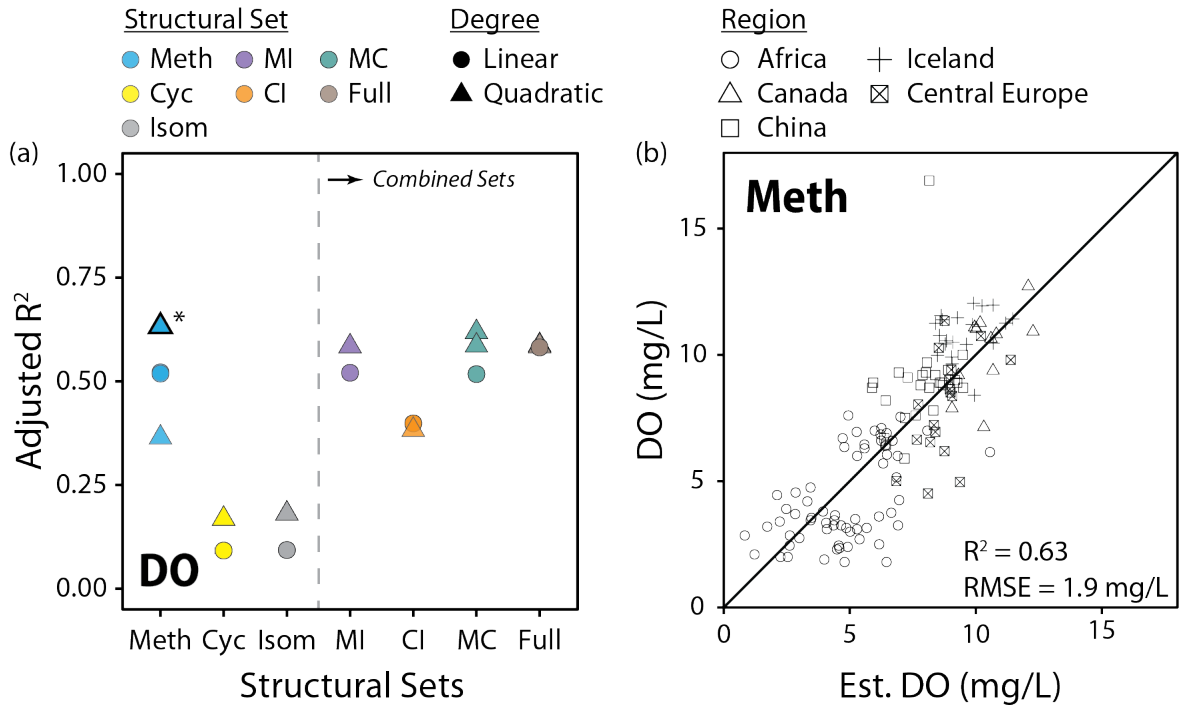

Figure S42. a) Performance (adjusted R2) of all linear and quadratic fits for mean lake water dissolved oxygen concentrations and brGDGT fractional abundances (FAs) calculated within the basic (Meth, Cyc, Isom; left of dashed line) and combined (Meth-Isom (MI), Cyc-Isom (CI), Meth-Cyc (MC), and Full sets; right of dashed line) structural sets. Results of both the SFS/SBE and combinatoric fitting methods are plotted. The highest performing fit (Meth set, quadratic, SFS/SBE) is bolded and marked with an asterisk in a) and plotted in b). "Est. DO" is the mean dissolved oxygen concentration estimated using this top fit.

Env. Variable	Subset	Adj. R^2	RMSE[a]	Variables	Compounds
MAF (°C)	**Full**	**0.91**	**1.97**	**6**	**15**
	MC	0.91	1.99	4	15
	MI	0.90	2.14	4	15
	Meth	**0.90**	**2.14**	**8**	**9**
	MI_a	0.90	2.18	4	5
	MBT'_{5Me}	0.89	2.32	1	7
	$Meth_a$	0.88	2.33	3	3
	$Meth_b$	0.79	3.10	5	5
	$Meth_c$	0.74	3.32	4	5
MST (°C)	Full	0.90	2.44	8	15
SWI (°C)	MC	0.89	30.13	6	15
WMT (°C)	Full	0.88	2.70	8	15
MAT (°C)	MI	0.87	3.44	9	15
ln(Conductivity)	**CI**	**0.83**	**0.66**	**7**	**15**
	MC	0.83	0.65	12	15
	Full	0.81	0.69	8	15
	MI	0.80	0.70	7	15
	Isom	0.76	0.78	6	8
	CI_{III}	0.75	0.80	3	6
	CI_{II}	0.73	0.84	4	6
	IR_{6Me}	0.66	0.95	1	12
	CI_I	0.65	0.95	4	3
pH	Full	0.74	0.55	8	15
	CI	**0.73**	**0.57**	**2**	**9**
	CI_{II}	0.68	0.62	3	6
	CBT	0.64	0.66	1	6
	CI_{III}	0.62	0.67	2	6
	CI_I	0.60	0.69	1	3
DO_{mean} (mg/L)	Meth	0.63	1.86	8	15
ln(Surface Area/Depth)	Full	0.59	2.26	7	15
ln(Volume)	Full	0.55	2.55	10	15
DO_{min} (mg/L)	Cyc_{III}	0.55	2.43	3	6
ln(Depth)	MI	0.35	1.02	6	15

Table S3. Summary of calibrations for all environmental variables (Env. Variable). "Variables" is the number of fitting variables used in each calibration. "Compounds" is the total number of compounds used in each calibration, including all those employed in fractional abundance calculations. Recommended fits are emphasized in bold. aRMSE units are indicated in the "Env. Variable" column.

In addition to those in the main text, we provide equations for the subset-specific $Meth_a$ + $Meth_b$, $Meth_a$, $Meth_b$, and $Meth_c$ MAF fits:

$$MAF\ (°C) = 85.02(\pm16.18) + 57.57(\pm15.83) \times fIb^2_{Meth} - 116.01(\pm31.14) \times fIb_{Meth} - 29.5(\pm5.58) \times fIIa^2_{Meth} - 66.06(\pm17.69) \times fIIb^2_{Meth} + 21.94(\pm7.89) \times fIIIa^2_{Meth} - 41.22(\pm6.04) \times fIIIa_{Meth} - 4.42(\pm1.44) \times fIIIb'^2_{Meth} - 69.4(\pm19.43) \times fIIIb_{Meth}\ (n = 182, R^2 = 0.89, RMSE\ =\ 2.19°C) \quad (S1)$$

$$MAF\ (°C) = 26.56(\pm0.52) - 34.67(\pm5.14) \times fIIa^2_{Meth} + 29.4(\pm7.46) \times fIIIa^2_{Meth} - 49.43(\pm4.92) \times fIIIa_{Meth}\ (n = 182, R^2 = 0.88, RMSE\ =\ 2.33°C) \quad (S2)$$

$$MAF\ (°C) = 79.72(\pm21.83) + 103.96(\pm19.08) \times fIb^2_{Meth} - 147.29(\pm40.62) \times fIb_{Meth} - 80.14(\pm23.81) \times fIIb^2_{Meth} - 7.19(\pm1.98) \times fIIIb'^2_{Meth} - 89.73(\pm26.54) \times fIIIb_{Meth}(n = 182, R^2 = 0.79, RMSE = 3.10°C) \quad (S3)$$

$$MAF\ (°C) = 9.38(\pm1.97) + 19.92(\pm2.41) \times fIc^2_{Meth} - 8.44(\pm2.89) \times fIIc_{Meth} + 18.83(\pm5) \times fIIIc'^2_{Meth} - 18.4(\pm3.32) \times fIIIc'_{Meth}(n = 157, R^2 = 0.74, RMSE = 3.32°C) \quad (S4)$$

We also provide the subset-specific CI_I, CI_{II}, and CI_{III} fits for conductivity,

$$ln(Cond.) = -20.07(\pm4.33) + 22.13(\pm4.34) \times fIa^2_{CI} - 61(\pm10.22) \times fIb^2_{CI} + 73.24(\pm10.93) \times fIb_{CI} + 123.55(\pm26.57) \times fIc^2_{CI}(n = 143, R^2 = 0.65, RMSE = 0.95) \quad (S5)$$

$$ln(Cond.) = 7.11(\pm0.82) + 5.17(\pm1.97) \times fIIa^2_{CI} - 9.42(\pm2.25) \times fIIa_{CI} - 38.77(\pm14.13) \times fIIb'^2_{CI} + 14.36(\pm4.83) \times fIIb'_{CI}(n = 143, R^2 = 0.73, RMSE = 0.84) \quad (S6)$$

$$ln(Cond.) = 7.46(\pm0.24) - 5.28(\pm0.32) \times fIIIa_{CI} - 268.59(\pm82.68) \times fIIIb^2_{CI} + 31.22(\pm7.74) \times fIIIb_{CI}(n = 143, R^2 = 0.75, RMSE = 0.80) \quad (S7)$$

and for pH,

$$pH = 5.96(\pm0.12) + 7.68(\pm0.5) \times fIb_{CI}(n = 154, R^2 = 0.60, RMSE = 0.69) \quad (S8)$$

$$pH = 8.31(\pm0.25) - 3.37(\pm0.28) \times fIIa_{CI} - 23.45(\pm7.59) \times fIIb^2_{CI} + 10.34(\pm2.38) \times fIIb_{CI}(n = 154, R^2 = 0.68, RMSE = 0.62) \quad (S9)$$

$$pH = 8.41(\pm0.13) - 2.84(\pm0.22) \times fIIIa^2_{CI} + 7.48(\pm2.37) \times fIIIb_{CI}(n = 154, R^2 = 0.62, RMSE = 0.67) \quad (S10)$$

Finally, we provide the highest-performing DO_{mean} calibration:

$$DO_{mean}\ (mg/L) = 7.6(\pm2.32) - 12.03(\pm2.6) \times fIa^2_{Meth} - 2.1(\pm0.74) \times fIc^2_{Meth} - 28.66(\pm8.5) \times fIIIa'^2_{Meth} + 31.09(\pm8.66) \times fIIIa'_{Meth} + 36.85(\pm8.37) \times fIIIa^2_{Meth} - 35.89(\pm7.93) \times fIIIa_{Meth} - 15.29(\pm3.44) \times fIIIb'^2_{Meth} + 15.82(\pm2.55) \times fIIIb'_{Meth}\ (n = 140, R^2 = 0.63, RMSE\ =\ 1.86\ mg/L) \quad (S11)$$

Other calibration equations are available upon request.

Literature Cited:

Naafs, B. D. A., Gallego-Sala, A. V., Inglis, G. N. and Pancost, R. D.: Refining the global branched glycerol dialkyl glycerol tetraether (brGDGT) soil temperature calibration, Org. Geochem., 106, 48–56, doi:10.1016/j.orggeochem.2017.01.009, 2017.
Russell, J. M., Hopmans, E. C., Loomis, S. E., Liang, J. and Sinninghe Damsté, J. S.: Distributions of 5- and 6-methyl branched glycerol dialkyl glycerol tetraethers (brGDGTs) in East African lake sediment: Effects of temperature, pH, and new lacustrine paleotemperature calibrations, Org. Geochem., 117, 56–69, 2018.
Stillwell, W.: Basic Membrane Properties of the Fluid Mosaic Model, in An Introduction to Biological Membranes, pp. 135–180, Elsevier., 2016.
Yao, Y., Zhao, J., Vachula, R. S., Werne, J. P., Wu, J., Song, X. and Huang, Y.: Correlation between the ratio of 5-methyl hexamethylated to pentamethylated branched GDGTs (HP5) and water depth reflects redox variations in stratified lakes, Org. Geochem., 147, 104076, doi:10.1016/j.orggeochem.2020.104076, 2020.